Journal of Power Sources 199 (2012) 124–131

Contents lists available at SciVerse ScienceDirect

Journal of Power Sources

journal homepage: www.elsevier.com/locate/jpowsour

Nanoporous PdCu alloy for formic acid electro-oxidation

Caixia Xu[a,*], Yunqing Liu[a], Jinping Wang[a], Haoran Geng[a], Huajun Qiu[b,c,*]

[a] School of Chemistry and Chemical Engineering, University of Jinan, Jinan 250022, Shandong Province, China
[b] School of Chemistry and Chemical Engineering, Shandong University, Jinan 250100, Shandong Province, China
[c] Qingdao Institute of Bioenergy and Bioprocess Technology, Chinese Academy of Sciences, Qingdao 266101, China

ARTICLE INFO

Article history:
Received 23 August 2011
Received in revised form 16 October 2011
Accepted 19 October 2011
Available online 25 October 2011

Keywords:
Palladium/copper alloy
Dealloying
Electrocatalyst
Fuel cell

ABSTRACT

In this work, nanoporous PdCu alloys (np-PdCu) with predetermined bimetallic ratios are fabricated by selectively dealloying PdCuAl ternary alloys in 1.0 M NaOH solution. Electron microscope and X-ray diffraction characterizations show that the nanoporous metals have three-dimensional bicontinuous ligament-pore structure with uniform ligament size. Electrochemical measurements demonstrate that np-PdCu has greatly enhanced electrocatalytic activity and structure stability towards formic acid oxidation (FAO) compared with nanoporous Pd (np-Pd). The surface specific activities of the nanoporous metals follow the order that np-$Pd_{50}Cu_{50}$ > np-$Pd_{75}Cu_{25}$ > np-$Pd_{30}Cu_{70}$ > np-Pd. The peak current density on np-$Pd_{50}Cu_{50}$ shows the highest value, which is about six times of that on np-Pd. The alloy ratio also has a significant effect on the electrocatalytic behavior of the PdCu alloy towards FAO. When the Cu content is lower than 50 at.%, the FAO is mainly through the direct pathway; when the Cu content reaches 70 at.%, the FAO through the CO pathway increases. Moreover, electrochemical stripping experiment and continuous potential scan demonstrate that np-$Pd_{50}Cu_{50}$ has a better resistance to CO poisoning and enhanced structure stability compared with other alloy samples. These results indicate the potential application of the np-$Pd_{50}Cu_{50}$ in direct formic acid fuel cell.

1. Introduction

Electrochemical oxidation of formic acid has attracted increasing attention due to the great potential in direct formic acid fuel cell (DFAFC) applications [1–3]. Recently, Pd-based catalysts were found to possess superior performances towards formic acid oxidation (FAO) compared with Pt-based catalysts [4–8]. It is generally accepted that formic acid molecules are oxidized on Pd catalysts in line with a direct dehydrogenation reaction mechanism to form CO_2 with less CO-like poisoning species generated, which is different from that of Pt catalysts with the main self-poisoning dehydration reaction pathway [4–8]. Therefore, considerable efforts have been made to develop a variety of Pd catalysts towards FAO [9–13]. It has also been demonstrated that combination of a second component (such as Pt, Au, Co, Ir, etc.) with Pd is an effective strategy to further enhance its catalytic activity [14–17]. The enhancement is mainly due to the weakening of the adsorption of inhibiting reaction intermediates on catalyst surface, which has been explained by the electronic, strain, or alloying effects [18,19]. However, the combination of a non-noble metal component which can enhance both the catalytic activity and stability of Pd is still challenging.

Recently, it has been demonstrated that Cu as an assistant component plays an important role for the enhancement of the catalytic activity of noble metals such as Pt and Pd [20–26]. Based on a series of experimental and theoretical studies, Mavrikakis et al. [20] proposed that the Pt/Cu near surface alloy is a promising catalyst for low-temperature water–gas-shift reaction due to the reduced CO surface binding energy. Zhou et al. [21] observed a high catalytic activity of Cu–Pt core–shell nanoparticles for NO reduction where they considered that the most active phase of the catalysts had Cu preferentially located in the sub-surface layers. Strasser et al. [22,23] reported that dealloyed Pt/Cu alloy nanoparticles (a Pt shell and PtCu alloy core nanostructure) exhibited an excellent activity for oxygen reduction reaction (ORR). Wang and Lu reported the effects of different Cu precursors on the microstructures of the formed PdCu alloy nanoparticles and their catalytic activities for CO oxidation [24]. It was observed that for the PdCu alloy obtained by using $CuCl_2$ as Cu precursor, Pd species would segregate on the particle surface, which results in higher catalytic activity [24]. The enhanced electrocatalytic activities of PdCu alloys for ORR and methanol oxidation have also been reported [25–27]. The results mentioned above indicate that Pd(Pt)Cu alloys with Pd(Pt) rich shell and alloy core have enhanced catalytic activities compared with pure Pd(Pt). On the other hand, the high catalytic

* Corresponding authors.
E-mail address: qiuhuajun@gmail.com (H. Qiu).

0378-7753/$ – see front matter © 2011 Elsevier B.V. All rights reserved.
doi:10.1016/j.jpowsour.2011.10.075

activity for CO oxidation and weak metal–CO band strength indicate that PdCu alloy may be a good electrocatalyst for FAO through the direct dehydrogenation pathway. For the preparation of Cu-based alloy nanomaterials, however, they are usually prepared by wet-chemical process with the excessive use of surfactant and organic chemicals at high temperatures. Besides, it is hard to control both the morphology and the alloy ratio of the alloy nanomaterials simultaneously during the metal salts reduction process.

Recently, dealloying of alloys has been demonstrated to be very powerful in generating three-dimensional (3D) bicontinuous nanoporous metal materials [27–33]. When used as catalyst, nanoporous metal materials have some advantages compared with metal nanoparticles: (1) it is free of particle agglomeration and can be easily employed; (2) prepared in concentrated acidic or alkaline solution (without any surfactants), the surface of the nanoporous metals is extremely clean; (3) prepared by simple dealloying instead of metal salts reduction, this method can achieve a nearly 100% yield with essentially no precious metal loss. Using the dealloying strategy, nanoporous PdCu alloys (np-PdCu) have been successfully prepared in our previous work, which shows remarkably enhanced electrocatalytic activity towards the oxidation of organic small molecules compared with np-Pd [27]. However, the effect of alloy ratio on the electrocatalytic activity of the np-PdCu alloy is still lacking.

In this work, np-PdCu alloys with different alloy ratios are fabricated by selectively dealloying PdCuAl ternary alloys. It is interesting to find that the alloy ratio has a significant effect on both the catalytic activity and behavior (the pathway of FAO) of the alloy catalyst. With remarkably improved catalytic activity and stability, np-$Pd_{50}Cu_{50}$ holds great promise as anode catalysts in DFAFC.

2. Experimental

PdCuAl alloy foils (~50 μm in thickness) were made by refining pure Pd, Cu, and Al (>99.9%) at high temperatures in an arc furnace under the protection of argon, followed by melt-spinning as reported in our previous work [27]. Al atomic content in all alloy foils was controlled to be 80 at.%. The atomic ratio between Pd and Cu is 3:1 (namely $Pd_{15}Cu_5Al_{80}$), 1:1 (namely $Pd_{10}Cu_{10}Al_{80}$) and 1:3 (namely $Pd_6Cu_{14}Al_{80}$). All the nanoporous metals were prepared by dealloying the alloy foils in 1 M NaOH solution for 24 h.

The catalyst ink was made by sonicating a mixture of 2.0 mg nanoporous metal catalysts powder, 1.0 mg carbon powder, 300 μL isopropanol, and 100 μL Nafion solution (5 wt.%) for 30 min. The catalyst ink (4 μL) was placed on a polished glassy carbon electrode (GCE, 4 mm in diameter) and dried. Prior to each measurement, the electrolytes were deoxygenated with high-purity N_2 for at least 30 min. Considering that Cu atoms on np-PdCu surface may be unstable in acid electrolytes, all the electrocatalytic measurements were recorded after the modified electrodes reached the steady state in 1.0 M H_2SO_4 solution by continuous cyclic voltammetry scanning from 0 to 1.35 V vs. RHE (namely pretreatment). All electrochemical measurements were performed on a CHI 760C electrochemical workstation. A three-electrode system was used with a modified GCE as working electrode, a Pt foil as counter electrode, and a mercury sulfate electrode (MSE) as reference electrode. All potentials were referred to RHE unless otherwise specified. The current densities were normalized by both the active surface area and mass of Pd. The electrochemical active surface areas (EASA) of the Pd-based electrodes were calculated based on literature [34]. EASA (cm^2) ≈ Charge/424, where Charge is obtained by integrating the charge associated with Pd oxide reduction and 424 μC cm^{-2} is the palladium's conversion factor [34].

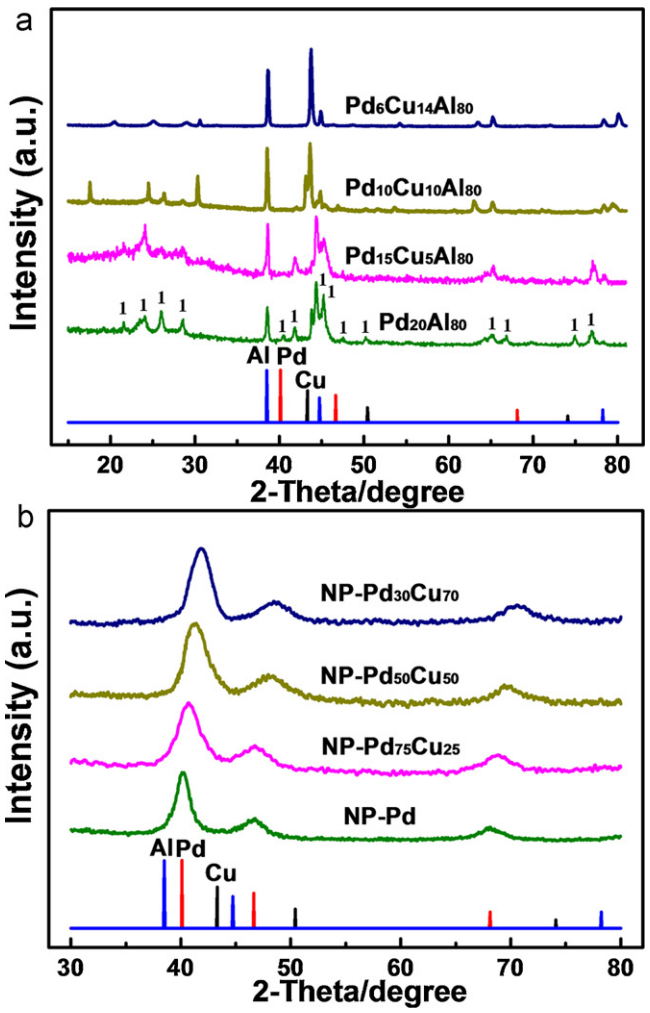

Fig. 1. XRD patterns of PdCuAl and PdAl alloys before (a) and after (b) dealloying. For comparison, the standard patterns of Pd, Cu and Al are also attached. The dealloying was carried out in 1 M NaOH aqueous solution for 24 h at room temperature.

Powder X-ray diffraction (XRD) data were collected on a Bruker D8 advanced X-ray diffractometer using Cu Kα radiation (λ = 1.5418 Å) at a scan rate of 0.04° s^{-1}. The micro-structures of all samples were characterized on a JEOL JSM-6700F field emission scanning electron microscope (SEM) equipped with an Oxford INCA X-sight energy dispersive X-ray spectrometer (EDS), and a JEM-2100 high-resolution transmission electron microscope (TEM). Surface composition and property of np-PdCu alloys were analyzed with an ESCALab250 X-ray photoelectron spectroscopy (XPS).

3. Results and discussion

3.1. Preparation and characterization of the prepared nanoporous alloys

Considering the more active property and rich supply of Al, Al-based alloys were chosen as the precursor alloys. The nominal compositions of the precursor alloys are $Pd_{20}Al_{80}$, $Pd_{15}Cu_5Al_{80}$, $Pd_{10}Cu_{10}Al_{80}$, and $Pd_6Cu_{14}Al_{80}$, which are predetermined by controlling the initial feed ratio and further confirmed by compositional analysis with EDS. Fig. 1a shows the XRD patterns of all precursor alloys. Upon detailed analysis, the PdAl alloy is composed of Al and Al_3Pd (denoted as 1) phases. The diffraction pattern of $Pd_{15}Cu_5Al_{80}$ alloy is similar to that of PdAl alloy.

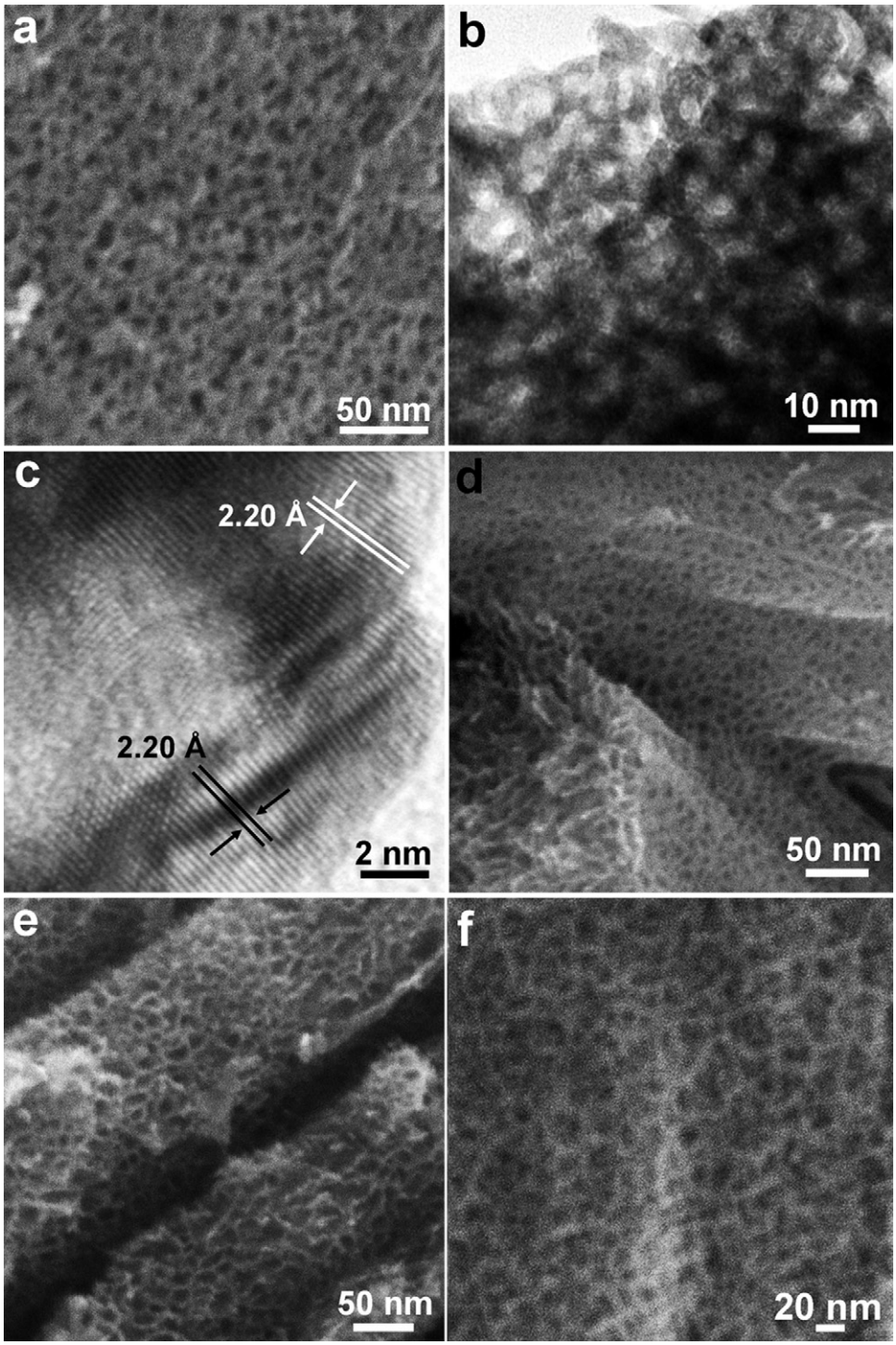

Fig. 2. SEM (a), TEM (b) and HRTEM (c) images of np-$Pd_{75}Cu_{25}$; SEM images of np-$Pd_{50}Cu_{50}$ (d), np-Pd (e) and np-$Pd_{30}Cu_{70}$ (f).

Most of the diffraction peaks can also be ascribed to Al and Al_3Pd alloy phases. When the Cu content further increases, the diffraction patterns of the precursor alloy change obviously, indicating the formation of Cu-based alloy phase such as CuAl phase. The complicated diffraction patterns of PdCuAl alloys suggest the existence of multiple alloy phases. Interestingly, as discussed below, although multiple alloy phases exist in the alloys, a uniform single-phase PdCu alloy and pure Pd can be formed after dealloying.

When the alloys are etched in 1 M NaOH solution at room temperature, Al can be easily and selectively removed. Fig. 1b shows the XRD patterns of the resulted nanoporous metals after dealloying. For np-Pd, the three diffraction peaks around 40.1, 46.7, and 68.1 (2θ) are in good agreement with those of standard diffractions from face-centered cubic (fcc) pure Pd as denoted by the dotted line, indicating the removal of Al. For each of the three np-PdCu alloys, there are also three diffraction peaks emerged, which are located between the projected 2θ values for pure Pd and Cu, indicating

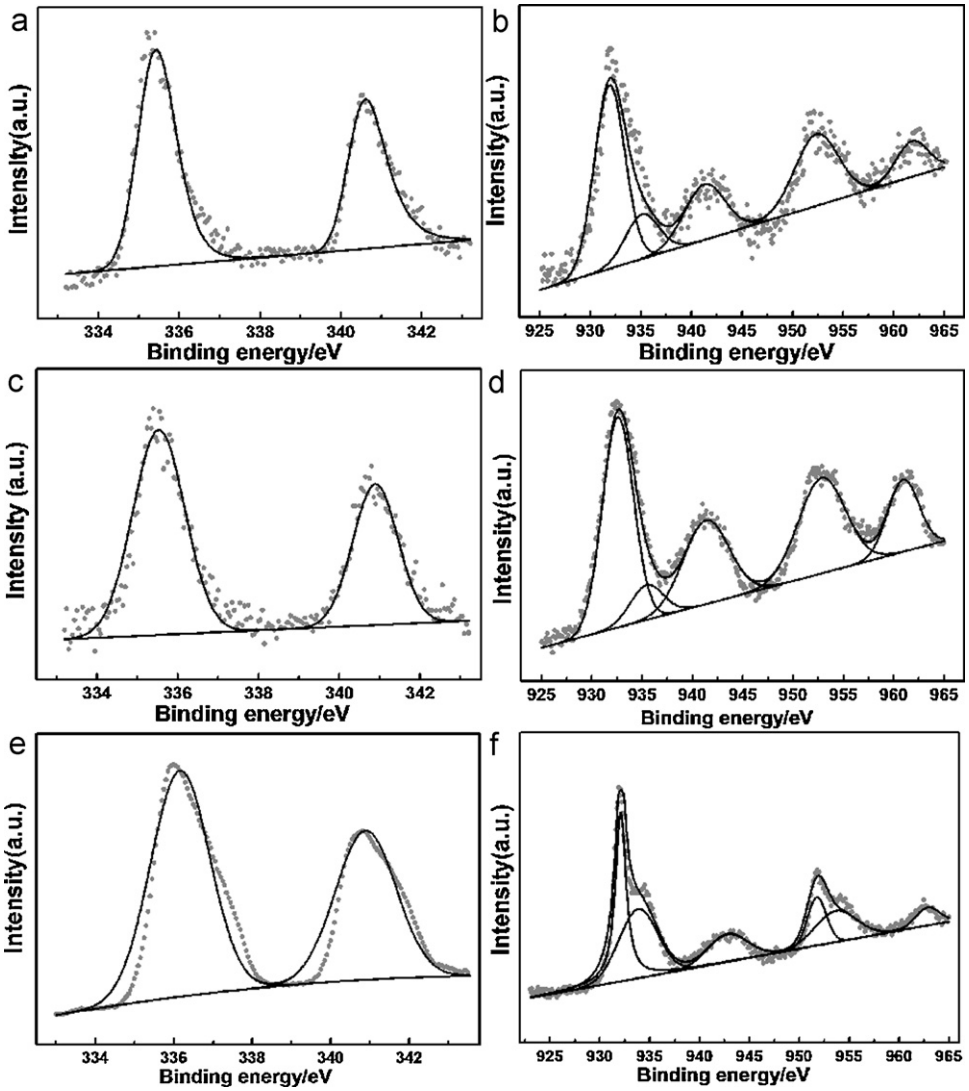

Fig. 3. XPS spectra of Pd 3d (a, c and e) and Cu 2p (b, d and f) for np-$Pd_{75}Cu_{25}$ (a and b), np-$Pd_{50}Cu_{50}$ (c and d) and np-$Pd_{30}Cu_{70}$ (e and f).

the formation of single-phase uniform fcc PdCu alloy structure. No diffraction peaks related to pure Pd, Cu, or their oxides are observed. By comparison with np-Pd, the diffraction peaks of np-PdCu alloys shift to higher angles with an increase in Cu content because of the substitution of smaller Cu atoms for Pd.

Fig. 2a shows the SEM image of the resulted sample upon dealloying of $Pd_{15}Cu_5Al_{80}$ in 1 M NaOH solution for 24 h at room temperature. It was observed that the obtained np-$Pd_{75}Cu_{25}$ has an open bicontinuous spongy-like morphology with a narrow ligament (i.e., the interconnected elongate alloy particles) size at ~6 nm. Fig. 2b gives the corresponding TEM image, in which the color contrast between the dark ligaments and bright pores further indicates the formation of three-dimensional (3D) bicontinuous interpenetrating ligament/pore structure. Fig. 2c provides a high-resolution TEM (HRTEM) image of the sample, where the continuous ordered lattice fringes are well resolved. The lattice spacing across the ligament is calculated to be ~0.220 nm, corresponding to the distance of the (1 1 1) crystal plane of fcc $Pd_{75}Cu_{25}$ alloy. This value is in excellent agreement with the value (0.220 nm) calculated by Vegard's law. These electron spectroscopy characterizations demonstrate that during dealloying of PdCuAl ternary alloy, as Al is leached away, the remained Pd and Cu atoms can inter-diffuse at the solution/solid interface and self-assemble to form 3D bicontinuous nanoporous structure with uniform PdCu alloy ligaments. Fig. 2d and e shows the typical SEM images of the resulted samples by dealloying $Pd_{10}Cu_{10}Al_{80}$ and PdAl alloys, respectively, under the same conditions. As observed, the obtained np-$Pd_{50}Cu_{50}$ and np-Pd also have similar 3D bicontinuous structures with ligament size of ~6 nm. Fig. 2f shows the SEM image of np-$Pd_{30}Cu_{70}$ obtained by dealloying $Pd_6Cu_{14}Al_{80}$ alloy. It is observed that the ligament size of np-$Pd_{30}Cu_{70}$ (15 nm) is larger than that of other nanoporous PdCu alloys (~6 nm). It is generally recognized that the dealloying process involves the dissolution of the less noble element and the formation/coarsening of the nanoporous structure by surface diffusion of the nobler element. The diffusion rates of the nobler metals at the solution/alloy interface during the dealloying play key roles in determining the ligament size of the formed nanoporous metals. Nanoporous metals such as Pt and Pd with ultrafine ligaments (less than 10 nm) are usually formed during the dealloying due to the slow diffusion rate of Pt and Pd, while nanoporous Cu with large ligament size (more than 100 nm) is usually formed due to the fast diffusion rate of Cu [33]. Thus, when the Cu content is ≤50 at.%, the large amount of Pd can slow down the diffusion of Cu at the solution/alloy interface

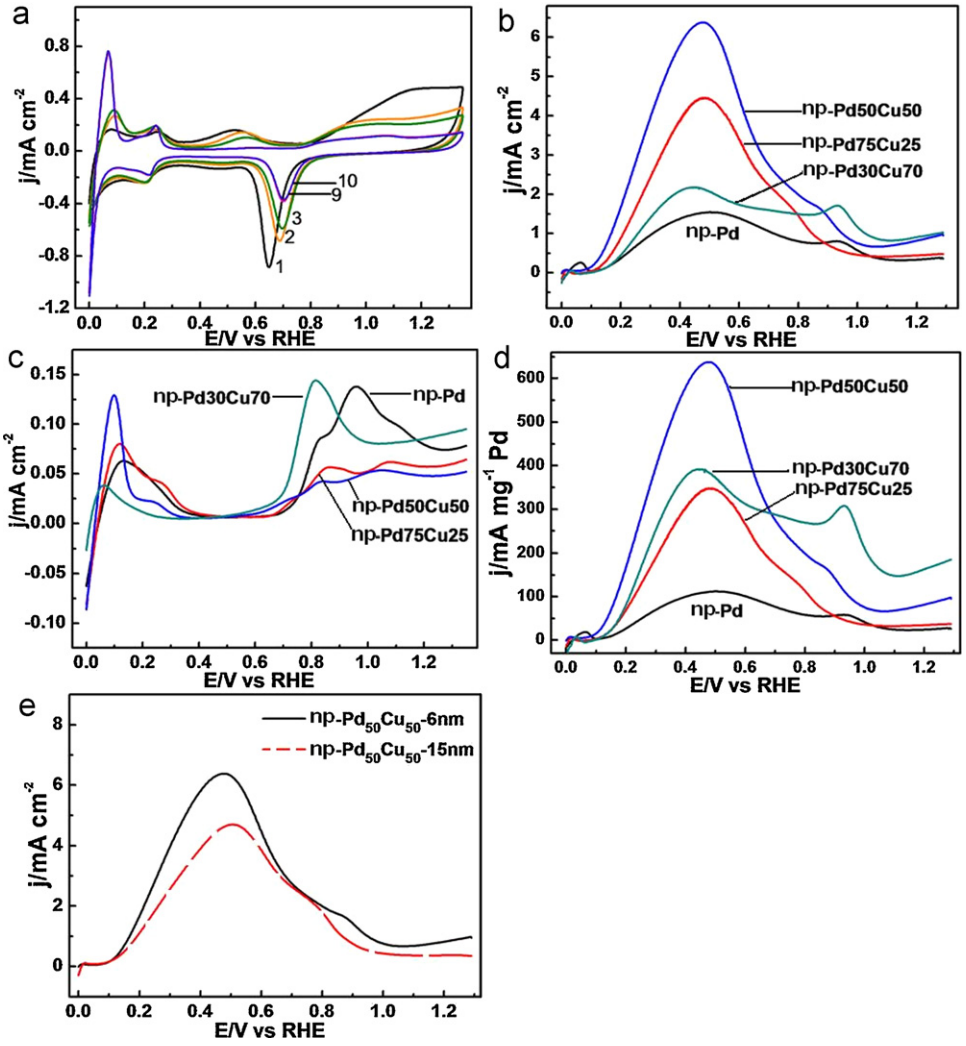

Fig. 4. CVs of np-$Pd_{75}Cu_{25}$ at different scan cycles in 1.0 M H_2SO_4 solution (a); LSVs of np-Pd and pretreated np-PdCu in 0.1 M $HClO_4$ + 0.1 M HCOOH solution (b); electrochemical stripping curves of the four samples after 1 h of FAO in 0.1 M $HClO_4$ + 0.1 M HCOOH solution under 0.1 V vs RHE (c); mass current densities of the four samples in 0.1 M $HClO_4$ + 0.1 M HCOOH solution (d); LSVs of np-$Pd_{50}Cu_{50}$ with different ligament sizes in 0.1 M $HClO_4$ + 0.1 M HCOOH solution (e). Scan rate: 50 mV s^{-1}.

forming np-PdCu with ultrafine ligaments. When the Cu content further increases to 70 at.%, the slow-down effect of Pd (30 at.%) decreases, resulting in np-PdCu with a relatively larger ligament size.

It is worth mentioning that the ligament/pore size of the nanoporous alloys is also depended on the dealloying time. For example, by extending the dealloying time from 24 to 48 h, the ligament size of np-$Pd_{50}Cu_{50}$ increased from ~6 nm to ~15 nm (figure not shown). This phenomenon is due to the fact that after the removal of Al, the surface atoms (Pd and Cu) can still diffuse along the solution/alloy interface when the porous alloy surface is in contact with the electrolyte. Thus, the ligament/pore size can be tuned by simply adjusting the dealloying time.

XPS is further used to examine the surface properties of np-PdCu. The binding energies of Pd $3d_{5/2}$ region for $Pd_{75}Cu_{25}$ (Fig. 3a), $Pd_{50}Cu_{50}$ (Fig. 3c) and $Pd_{30}Cu_{70}$ (Fig. 3e) are located at 335.4, 335.6 and 336.0 eV, respectively, revealing a shift to higher binding energy with increasing Cu content, as compared with 335.1 eV for pure Pd [35]. The shift of the binding energy for Pd in np-PdCu could be ascribed to the charge transfer between them due to the formation of the PdCu alloy as demonstrated by XRD analysis. Fig. 3b, d and f shows the Cu 2p spectra for $Pd_{75}Cu_{25}$, $Pd_{50}Cu_{50}$ and $Pd_{30}Cu_{70}$, respectively. The spectra show the presence of both metal Cu (932.2 eV) and CuO (935.3 eV) which is characterized by the presence of a satellite signal at ~942.5 eV [35]. Note that some Cu_2O should also exist on the surface. However, it is hard to be discriminated from Cu due to their same binding energy.

3.2. Electrocatalytic activities of np-PdCu towards FAO

In this work, the electrocatalytic activities of np-PdCu alloys for FAO were examined to evaluate their potential value as anode catalysts in DFAFC. Fig. 4a shows the change of cyclic voltammograms (CVs) of np-$Pd_{75}Cu_{25}$ with increasing scan cycles in 1.0 M H_2SO_4 solution (pretreatment). At the first scan, np-PdCu alloys show a big anodic peak at 0.3–0.7 V, which is due to the oxidation of exposed Cu atoms on alloy surface [27]. This peak decreased with the increase of scan cycles and disappeared at the ninth cycle. Meanwhile, the peaks for the reduction of metal oxides at ca. 0.65 V shifted positively and the peaks for hydrogen adsorption/desorption at 0–0.3 V increased with the increase of scan cycles. After the ninth scan, the CV of np-PdCu was the same as that of np-Pd and changed negligibly with further scan. These results indicate the dissolution of Cu on the alloy surface and formation of a nearly pure Pd-shell by the electrochemical pretreatment. Other

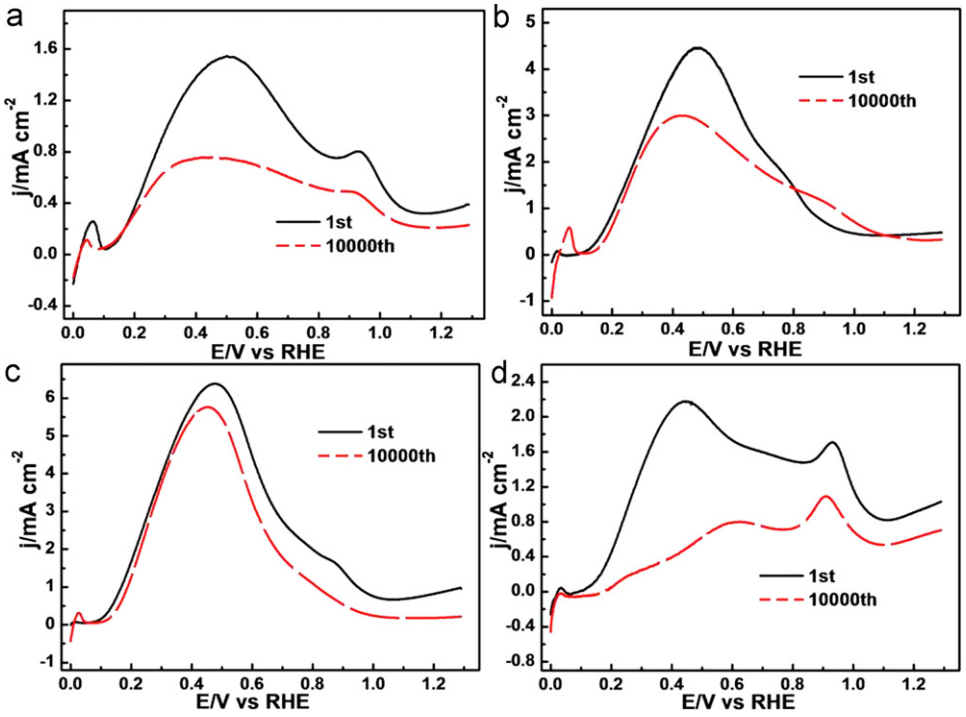

Fig. 5. LSVs of np-Pd (a), np-$Pd_{75}Cu_{25}$ (b), np-$Pd_{50}Cu_{50}$ (c) and np-$Pd_{30}Cu_{70}$ (d) in 0.1 M $HClO_4$ + 0.1 M HCOOH solution before and after long-term potential cycles from 0.6 to 0.9 V in 0.1 M $HClO_4$ solution. Scan rate: 50 mV s^{-1}.

PdCu alloy samples have similar electrochemical behaviors as that of np-$Pd_{75}Cu_{25}$ during the pretreatment except that as the Cu content increases, the peak for the exposed Cu oxidation becomes larger and more scan cycles are needed for the alloy samples to reach the electrochemical steady state. It should be mentioned that after the electrochemical pretreatment, the Cu content only slightly decreases, i.e., only Cu on the surface site is dissolved [27].

Fig. 4b shows the linear sweep voltammograms (LSVs) of np-Pd and np-PdCu in 0.1 M $HClO_4$ solution containing 0.1 M HCOOH. For all the four catalysts, a large current peak at 0.2–0.8 V and a small shoulder peak at 0.8–1.0 V are observed, which corresponded to the oxidation of FAO via the direct pathway and the CO pathway, respectively [4–8,36–39]. For the peak at 0.2–0.8 V, the order of surface specific current densities at the four electrocatalysts is np-Pd < np-$Pd_{30}Cu_{70}$ < np-$Pd_{75}Cu_{25}$ < np-$Pd_{50}Cu_{50}$. The highest current density at np-$Pd_{50}Cu_{50}$ indicates the highest electrocatalytic activity of np-$Pd_{50}Cu_{50}$ towards FAO. For the oxidation peak at 0.8–1.0 V, the peaks at np-$Pd_{75}Cu_{25}$ and np-$Pd_{50}Cu_{50}$ are indistinct, indicating the FAO at these two alloys are mainly through the direct pathway. However, the peak at np-$Pd_{30}Cu_{70}$ is much larger (almost comparable with the peak at 0.2–0.8 V), indicating that more formic acid is oxidized through the CO pathway when the content of Cu reaches to 70 at.%. This result also indicates that the ratio of Pd and Cu has a significant effect on the electrocatalytic behaviors of the nanostructured PdCu alloy, i.e., the electrocatalytic activity towards FAO via the direct pathway increases as the Cu content increase to 50 at.% and then decreases as the Cu content reaches to 70 at.%. To further demonstrate the conclusion, electrochemical stripping experiment was carried out. Fig. 4c shows the electrochemical stripping curves of the four samples in 0.1 M $HClO_4$ solution after 1 h of FAO under 0.1 V in 0.1 M $HClO_4$ + 0.1 M HCOOH solution. It can be clearly observed that the stripping current densities at np-$Pd_{50}Cu_{50}$ and np-$Pd_{75}Cu_{25}$ are much smaller, indicating that FAO at these two samples are mainly through the direct pathway with less CO produced. The np-$Pd_{30}Cu_{70}$ sample generates the highest stripping current density at a relatively negative potential, indicating that more FAO are through the CO pathway at np-$Pd_{30}Cu_{70}$. np-Pd also exhibits a high current density at a slightly more positive potential. The negatively shifted peak potential on np-PdCu indicates that the adsorption of CO on np-PdCu is weak compared with that on np-Pd, which is in good agreement with results obtained elsewhere [19]. The weak CO adsorption should be due to the electronic or structure modification of Pd by alloying with Cu [20]. The weak adsorption of CO-like reaction intermediate also explains why PdCu alloys have higher electrocatalytic activities for FAO.

For practical applications, the evaluation of mass specific activity of noble metal is also very important. Fig. 4d shows the Pd mass specific activities of the as-prepared PdCu alloys in 0.1 M $HClO_4$ + 0.1 M HCOOH solution. It is found that np-$Pd_{50}Cu_{50}$ also has the highest mass specific activity. Although, the surface specific activity of np-$Pd_{70}Cu_{30}$ is quite low, its mass specific activity is slightly higher than that of np-$Pd_{75}Cu_{25}$ due to the low content of Pd in the $Pd_{70}Cu_{30}$ sample. It is also clear that all the alloy samples have much higher mass specific activity compared with np-Pd.

The effect of the ligament size on the FAO activity was also tested with np-$Pd_{50}Cu_{50}$ as the representative. As shown in Fig. 4e, the current density of FAO on the sample with a ligament size of ~6 nm is slightly higher than that on the sample with the ligament size of ~15 nm. This result indicates that np-PdCu with a smaller ligament size has a relatively higher electrocatalytic activity [39]. Thus, the lower catalytic activity of np-$Pd_{30}Cu_{70}$ as mentioned above should be partly attributed to its larger ligament size. Nevertheless, it is clear that the main reason for the remarkably decreased catalytic activity and changed electrocatalytic behavior of np-$Pd_{30}Cu_{70}$ is due to the change of alloy ratio because the change of ligament size from 6 to 15 nm only slightly affects the catalytic activity.

Besides the required high activity for electrocatalysts, the stability is also of importance for practical applications. Therefore, we further measured the stabilities of np-PdCu alloys by continuous cyclic potential scan from 0.6 to 0.9 V in 0.1 M $HClO_4$ solution. As shown in Fig. 5, after 10,000 potential cycles, the electrocatalytic activities of all the four samples decreased. In comparison,

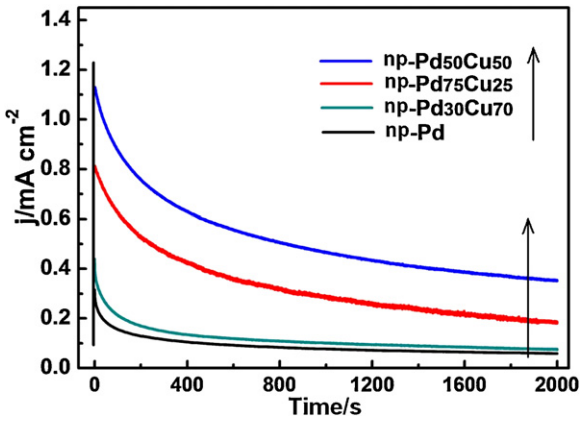

Fig. 6. Electrochemical potentiostatic currents for np-PdCu alloys and np-Pd in 0.1 M $HClO_4$ + 0.1 M HCOOH solution at 0.2 V vs RHE.

the decreased intensity of np-$Pd_{50}Cu_{50}$ is the lowest, indicating the best stability of this alloy sample. It is also interesting to observe that for the np-$Pd_{30}Cu_{70}$ sample, not only the current density is decreased, but also the shape of the curve changed. The peak at 0.2–0.8 V became much smaller (smaller than that at 0.8–1.0 V), indicating that as the potential cycle increases, the FAO on the np-$Pd_{30}Cu_{70}$ sample through the direct pathway decreases. The change of the catalytic behavior of the np-$Pd_{30}Cu_{70}$ sample should be due to the continuous potential cycling which rearranges the surface atoms. It is known that in acidic aqueous solutions, Pd atoms on the surface are removable during the electrochemical oxidation and reduction process. However, the real reason for the change of the catalytic behavior still needs further study.

Further evaluation of the catalytic durability was conducted by chronoamperometry. As shown in Fig. 6, at the beginning the potentiostatic currents decreased rapidly for all catalysts due to the formation of double layer capacitance. The following current decrease should originate from the loss of surface active sites caused by the adsorption of intermediate species on the catalyst surface [40,41]. The current densities at np-$Pd_{50}Cu_{50}$ and np-$Pd_{75}Cu_{25}$ are higher and decrease more slowly compared with that at np-$Pd_{30}Cu_{70}$ and np-Pd, which is due to the higher electrocatalytic activities and less CO poisoning of np-$Pd_{50}Cu_{50}$ and np-$Pd_{75}Cu_{25}$. This is in good agreement with the results obtained by linear sweep voltammetry and CO electrochemical stripping test as discussed above.

As to the origin of the enhanced performance of np-PdCu alloys, during potential scan in the acid solution, Cu atoms on np-PdCu surface are gradually dissolved, and the left Pd atoms will undergo a reconstruction process to form a nearly pure Pd shell with the residual Cu atoms buried within the sub-surface atomic layers. These sublayer Cu atoms may provide an electronic modification for the topmost Pd layer by a surface strain effect or alloying effect [42,43], which may provide unique surface sites for formic acid adsorption and subsequent electro-oxidation. It has also been demonstrated that the change of d-band center of metal catalysts can significantly influence their catalytic reaction kinetics by altering the adsorption energies of reaction intermediates [18]. By density functional theory (DFT) calculation, Fouda-Onana and Savadogo have reported that after the incorporation of Cu (from 0 to 50 at.%), the d-band center of Pd shifts to a lower value of −2.638 eV from −1.843 eV. When the Cu content reaches 75 at.%, the d-band center shifts to −2.798 eV [44]. The decreased d-band center would result in the weakening of CO adsorption and retaining the high activity of np-PdCu towards FAO [45]. However, based on the result obtained in this work (np-$Pd_{30}Cu_{70}$ has a much lower catalytic activity and different catalytic behavior), other factors such as morphology, surface state of alloy, etc. also play important roles in the overall catalytic activity.

4. Conclusions

Nanoporous PdCu alloys with uniform ligament size and controllable bimetallic ratio are straightforwardly fabricated by a simple dealloying process. Electrochemical measurements demonstrated that the incorporation of Cu greatly enhanced both the electrocatalytic activity and stability of the Pd-based nanoporous catalysts towards FAO. Especially, np-$Pd_{50}Cu_{50}$ shows superior catalytic activities and is more resistant to surface poisoning compared with other np-PdCu alloys and np-Pd. It was also demonstrated that the alloy ratio has a significant effect on the catalytic behavior of the nanoporous alloys. For np-$Pd_{75}Cu_{25}$ and np-$Pd_{50}Cu_{50}$, the FAO is mainly through the direct pathway. When the Cu content reaches 70 at.%, more formic acid are electroxidized via the CO pathway. These results indicate the potential application of the np-PdCu alloys in direct formic acid fuel cells. In addition, the present preparation strategy is simple, green, and applicable to large-scale synthesis.

Acknowledgements

This work was supported by the National Science Foundation of China (51001053, 50871047), and Natural Science Foundation of Shandong Province (ZR2010EQ039). H. Qiu thanks the two reviewers for their insightful advice.

References

[1] S. Ha, R. Larsen, Y. Zhu, R.I. Masel, Fuel Cells 4 (2004) 337–343.
[2] C. Rice, S. Ha, R.I. Masel, P. Waszczuk, A. Wieckowski, T. Barnard, J. Power Sources 11 (2002) 83–89.
[3] S. Ha, Z. Dunbar, R.I. Masel, J. Power Sources 158 (2006) 129–136.
[4] H. Miyake, T. Okada, G. Samjeské, M. Osawa, Phys. Chem. Chem. Phys. 10 (2008) 3662–3669.
[5] J. Wang, G. Yin, Y. Chen, R. Li, X. Sun, Int. J. Hydrogen Energy 34 (2009) 8270–8275.
[6] J. Jiang, A. Kucernak, J. Electroanal. Chem. 520 (2002) 64–70.
[7] J.D. Lovic, A.V. Tripkovic, S.L. Gojkovic, K.D. Popovic, D.V. Tripkovic, P. Olszewski, J. Electroanal. Chem. 581 (2005) 294–302.
[8] S. Ha, R. Larsen, R.I. Masel, J. Power Sources 144 (2005) 28–34.
[9] J. Ge, W. Xing, X. Xue, C. Liu, T. Lu, J. Liao, J. Phys. Chem. C 111 (2007) 17305–17310.
[10] H. Meng, S. Sun, J.P. Masse, J.P. Dodelet, Chem. Mater. 20 (2008) 6998–7002.
[11] V. Mazumder, S. Sun, J. Am. Chem. Soc. 131 (2009) 4588–4589.
[12] Y.W. Lee, J.K. Oh, H.S. Kim, J.K. Lee, S.B. Han, W. Choi, K.W. Park, J. Power Sources 195 (2010) 5896–5901.
[13] X.G. Wang, W.M. Wang, Z. Qi, C.C. Zhao, H. Ji, Z.H. Zhang, J. Power Sources 195 (2010) 6740–6747.
[14] D. Morales-Acosta, J. Ledesma-Garcia, L.A. Godinez, H.G. Rodriguez, L. Alvarez-Contreras, L.G. Arriaga, J. Power Sources 195 (2010) 461–465.
[15] X.G. Li, I.M. Hsing, Electrochim. Acta 51 (2006) 3477–3483.
[16] X. Wang, Y. Tang, Y. Gao, T.H. Lu, J. Power Sources 175 (2008) 784–788.
[17] Y. Liu, L.W. Wang, G. Wang, C. Deng, B. Wu, Y. Gao, J. Phys. Chem. C 114 (2010) 21417–21422.
[18] J.R. Kitchin, J.K. Norskov, M.A. Barteau, J.G. Chen, J. Chem. Phys. 120 (2004) 10240–10246.
[19] L. Dai, S. Zou, J. Power Sources 196 (2011) 9369–9372.
[20] J. Knudsen, A.U. Nilekar, R.T. Vang, J. Schnadt, E.L. Kunkes, J.A. Dumesic, M. Mavrikakis, F. Besenbacher, J. Am. Chem. Soc. 129 (2007) 6485–6490.
[21] S.H. Zhou, B. Varughese, B. Eichhorn, G. Jackson, K. McIlwrath, Angew. Chem. Int. Ed. 44 (2005) 4539–4543.
[22] P. Mani, R. Srivastava, P. Strasser, J. Power Sources 196 (2011) 666–673.
[23] S. Koh, P. Strasser, J. Am. Chem. Soc. 129 (2007) 12624–12625.
[24] F. Wang, G. Lu, Int. J. Hydrogen Energy 35 (2010) 7253–7260.
[25] F. Gobal, R. Arab, J. Electroanal. Chem. 647 (2010) 66–73.
[26] W.D. Kang, Y.C. Wei, C.W. Liu, K.W. Wang, Electrochem. Commun. 13 (2011) 162–165.
[27] C.X. Xu, A.H. Liu, H.J. Qiu, Electrochem. Commun. 13 (2011) 766–769.
[28] H.J. Qiu, Z.H. Zhang, X.R. Huang, Y.B. Qu, Chem. Phys. Chem. 12 (2011) 2118–2123.
[29] J.S. Yu, Y. Ding, C.X. Xu, A. Inoue, T. Sakurai, M.W. Chen, Chem. Mater. 20 (2008) 4548–4550.

[30] H.J. Qiu, L.Y. Xue, G.L. Ji, G.P. Zhou, X.R. Huang, Y.B. Qu, P.J. Gao, Biosens. Bioelectron. 24 (2009) 3014–3018.
[31] L.Y. Chen, L. Zhang, T. Fujita, M.W. Chen, J. Phys. Chem. C 113 (2009) 14195–14199.
[32] H.J. Qiu, L. Lu, X.R. Huang, Z.H. Zhang, Y.B. Qu, Bioresour. Technol. 101 (2010) 9415–9420.
[33] Z.H. Zhang, Y. Wang, Z. Qi, W.H. Zhang, J.Y. Qin, J. Frenzel, J. Phys. Chem. C 113 (2009) 12629–12636.
[34] W. Pan, X. Zhang, H. Ma, J. Zhang, J. Phys. Chem. C 112 (2008) 2456–2461.
[35] A.M. Venezia, L.F. Liotta, G. Deganello, Z. Schay, L. Guczi, J. Catal. 182 (1999) 449–455.
[36] Y.Z. Lu, W. Chen, J. Phys. Chem. C 114 (2010) 21190–21200.
[37] C. Du, M. Chen, W. Wang, G. Yin, ACS Appl. Mater. Interfaces 3 (2011) 105–109.
[38] N. Hoshi, K. Kida, M. Nakamura, M. Nakada, J. Phys. Chem. B 110 (2006) 12480–12484.
[39] W.J. Zhou, J.Y. Lee, J. Phys. Chem. C 112 (2008) 3789–3793.
[40] J. Prabhuram, T. Zhao, Z. Tang, R. Chen, Z. Liang, J. Phys. Chem. B 110 (2006) 5245–5252.
[41] A. Kabbabi, R. Faure, R. Durand, B. Beden, F. Hahn, J.M. Leger, C. Lamy, J. Electroanal. Chem. 444 (1998) 41–53.
[42] M. Abel, Y. Robach, L. Porte, Surf. Sci. 498 (2002) 244–256.
[43] A.U. Nilekar, Y. Xu, J. Zhang, M.B. Vukmirovic, K. Sasaki, R.R. Adzic, M. Mavrikakis, Top. Catal. 46 (2007) 276–284.
[44] F. Fouda-Onana, O. Savadogo, Electrochim. Acta 54 (2009) 1769–1776.
[45] V. Stamenkovic, B.S. Mun, K.J.J. Mayrhofer, P.N. Ross, N.M. Markovic, J. Rossmeisl, J. Greeley, J.K. Norskov, Angew. Chem. Int. Ed. 45 (2006) 2897–2901.